Maximum-Entropy Density Estimation for MRI Stochastic Surrogate Models

Zheng Zhang*, Niloofar Farnoosh*, Thomas Klemas, and Luca Daniel

***Abstract*—Stochastic spectral methods can generate accurate compact stochastic models for electromagnetic problems with material and geometric uncertainties. This letter presents an improved implementation of the maximum-entropy algorithm to compute the density function of an obtained generalized polynomial chaos expansion in Magnetic Resonance Imaging (MRI) applications. Instead of using statistical moments, we show that the expectations of some orthonormal polynomials can be better constraints for the optimization flow. The proposed algorithm is coupled with a finite element-boundary element method (FEM-BEM) domain decomposition field solver to obtain a robust computational prototyping for MRI problems with low and high dimensional uncertainties.**

***Index Terms*—Uncertainty quantification, electromagnetics, density function, magnetic resonance imaging (MRI).**

I. Introduction

THERE is an increasing interest for analyzing the geometric and material uncertainties in computational electromagnetics [1]–[4] using stochastic spectral methods [5]–[7]. Typical application examples include fast statistical analysis of specific absorption rate (SAR) in magnetic resonance imaging (MRI) [8], radar cross section in scattering applications [3], S-parameters in microwave circuits [4], and spectral characteristics in silicon photonic resonators [9]. Using much fewer samples than Monte Carlo, such techniques generate a truncated generalized polynomial-chaos expansion [5]–[7]:

$$y = g(\mathbf{x}) = \sum_{\boldsymbol{\alpha}\in\mathcal{P}} a_{\boldsymbol{\alpha}} \Psi_{\boldsymbol{\alpha}}(\mathbf{x}), \text{with } y \in \mathbb{R} \text{ and } \mathbf{x} \in \mathbb{R}^d \quad (1)$$

where the basis function $\Psi_{\boldsymbol{\alpha}}(\mathbf{x})$ is a multivariate orthonormal polynomial of random parameters $\mathbf{x} = [x_1, \cdots, x_d]$, and $a_{\boldsymbol{\alpha}} \in \mathbb{R}$ is the coefficient indexed by $\boldsymbol{\alpha} \in \mathbb{N}^d$. The details of constructing $\Psi_{\boldsymbol{\alpha}}$ can be found, for instance, in Section II of [10]. With the surrogate model in (1), designers can quickly obtain some important statistical metric (e.g., mean and variance) of y. However, it is nontrivial to extract certain information such as a closed-form probability density function.

This paper investigates how to construct a closed-form density function of y given a surrogate model in (1) for an MRI application. The results can be used for robust MRI coil design or for higher-level reliability analysis. Existing techniques in the circuit community includes moment matching [11] and the recently developed monotonic interpolation [12]. In this letter, we focus on the maximum entropy technique [13], since it provides the least biased estimation by avoiding anything unknown. Such technique was recently applied to extract the density function of analog circuits [14] using some statistical moment constraints. We show that such constraints may cause numerical instability, and thus we propose to use some orthonormal polynomials in the constraint functions. Such modifications bring in better numerical behaviors, which is verified both theoretically and numerically in this work.

The proposed algorithm is coupled with a FEM-BEM domain decomposition field solver to model stochastic MRI problems with low and high dimensional uncertainties. In MRI problems, the human body is illuminated by some radiation antennas in free space. The permittivity and conductivity of different tissues are subject to some uncertainties. In this letter, the interaction of electromagnetic waves with human tissues is characterized by computing the input impedance of the radiation sources. Our numerical results demonstrate the effectiveness of the proposed algorithm.

II. Preliminaries

A. Stochastic Electromagnetic Field Solver for MRI Problems

A FEM-BEM domain decomposition field solver is implemented to simulate deterministic MRI scattering problems consisting of several loop antennas placed around a human body [15]. In this approach, the whole computational domain is divided into two sub-domains, which are the set of loop antennas and the human body. The loop antenna sub-domain containing PECs is handled by BEM, implementing the standard electric field integral equation (EFIE). On the other hand, FEM is applied to human body sub-domain consist of different tissues with high contrast in electrical properties by solving the Helmholtz vector wave equation:

$$\nabla \times \mu_r^{-1} \nabla \times \vec{E}(x) - k_0^2 \varepsilon_r \vec{E}(x) + j\omega\mu_0\sigma\vec{E}(x) = 0 \quad (2)$$

where k_0 is the free space wave number, ε_r, μ_r are the relative permittivity and permeability and σ is the conductivity of different tissues in human body. FEM region is further decomposed into interior and exterior problems by defining dual cement variables on its surfaces ($\vec{j}^{\pm} = n^{\pm} \times \vec{H}$, $\vec{e}^{\pm} = n^{\pm} \times \vec{E} \times n^{\pm}$), where negative and positive sign corresponds to interior and exterior variables respectively and $n^{\pm}$ are unit vectors on the surface. Then, the Robin impedance boundary condition is applied at the interface to enforce the

* Z. Zhang and N. Farnoosh equally contributed to this work. This work was sponsored by the MIT-SkolTech program, the MIT-Italy Rocca program, the National Institute of Health, and the Assistant Secretary of Defense for Research and Engineering under Air Force Contract #FA8721-05-C-0002. Opinions, interpretations, conclusions and recommendations are those of the author and are not necessarily endorsed by the United States Government.

Z. Zhang, N. Farnoosh and L. Daniel are with the Research Laboratory of Electronics, Massachusetts Institute of Technology (MIT), Cambridge, MA 02139, USA. T. Klemas is with the MIT Lincoln Laboratory. (e-mail: z_zhang@mit.edu, nfarnoos@mit.edu, klemas@ll.mit.edu, luca@mit.edu).

continuity of electric and magnetic fields and to connect the interior and exterior problems as follows:

$$\vec{e}^{-} + \vec{j}^{-} = \vec{e}^{+} - \vec{j}^{+}, \quad \vec{e}^{-} - \vec{j}^{-} = \vec{e}^{+} + \vec{j}^{+}. \tag{3}$$

Finally, the overall solution of the problem is obtained by taking into account the mutual coupling between the two subdomains. Since the coupling computation is dominant in the whole solution of the system, a randomized SVD combined with discrete empirical interpolation [16] is employed to accelerate the computation [15].

In stochastic simulation, the developed MRI field solver is used as a black box. When the dimensionality of $\mathbf{x}$ is small, some testing points of $\mathbf{x}$ are selected according to [7]. Then for each sample the deterministic MRI solver is called to generate a sample solution for y. Finally, the generalized polynomial-chaos expansion (1) is obtained by interpolation [7]. For high-dimensional problems, we use the sparse stochastic testing simulator [17] to generate a representation for y. This simulator uses analysis of variance (ANOVA) to decompose y into some low-dimensional functions of the uncertainties $\mathbf{x}$, then the importance of each random parameter and the couplings among them are estimated on-the-fly, giving a sparse generalized polynomial-chaos expansion for y.

B. Maximum-Entropy Density Estimation

In maximum entropy, a probability density function $p(y)$ is obtained by solving the convex optimization problem:

$$\begin{aligned} \underset{p(y)}{\text{maxmize}} \quad & H\left(p(y)\right) \\ \text{subject to} \quad & \mathbb{E}\left(\phi_j(y)\right) = \mu_j,\ j = 0, \cdots, m \end{aligned} \tag{4}$$

where $\mathbb{E}\left(\phi_j(y)\right) = \int_{\Omega} \phi_j(y) p(y) dy$, $\mu_0 = 1$, $\phi_0(y) = 1$, and the entropy function $H\left(p(y)\right)$ is defined as

$$H\left(p(y)\right) := -\int_{\Omega} p(y) \ln\left[p(y)\right] dy. \tag{5}$$

Let $\boldsymbol{\phi}(y) := [\phi_0(y), \cdots, \phi_m(y)]^T$, and introduce the Lagrangian multipliers $\boldsymbol{\lambda} = [\lambda_0, \cdots, \lambda_m]^T$. It is well known that the solution to the above convex optimization (4) is

$$p(y) = \exp\left(-\boldsymbol{\lambda}^T \boldsymbol{\phi}(y)\right), \tag{6}$$

which provides $H\left(p(y)\right) = \int_{\Omega} \exp\left(-\boldsymbol{\lambda}^T \boldsymbol{\phi}(y)\right) \boldsymbol{\lambda}^T \boldsymbol{\phi}(y) dy$. Therefore, one only needs to compute $\boldsymbol{\lambda}$ which then uniquely determines $p(y)$ according to (6).

In order to obtain $\boldsymbol{\lambda}$, we solve the nonlinear equation

$$\mathbf{f}\left(\boldsymbol{\lambda}\right) = \left[f_0\left(\boldsymbol{\lambda}\right), \cdots, f_m\left(\boldsymbol{\lambda}\right)\right]^T = 0 \tag{7}$$

where $f_j\left(\boldsymbol{\lambda}\right) = \mathbb{E}\left(\phi_j(y)\right) - \mu_j$. Starting from an initial guess $\boldsymbol{\lambda}^0$, (7) is solved by Newton iterations

$$\text{solve } \mathbf{J}\left(\boldsymbol{\lambda}^l\right) \Delta\boldsymbol{\lambda} = -\mathbf{f}\left(\boldsymbol{\lambda}^l\right), \ \text{ update } \boldsymbol{\lambda}^{l+1} = \boldsymbol{\lambda}^l + \Delta\lambda$$

$k = 0, 1, 2, \cdots$ until convergence. The (j,k) element of the Jacobian matrix $\mathbf{J}\left(\boldsymbol{\lambda}\right) = \partial \mathbf{f} / \partial \boldsymbol{\lambda}$ is

$$\mathbf{J}_{j,k}\left(\boldsymbol{\lambda}\right) = -\int_{\Omega} \phi_{j-1}(y) \phi_{k-1}(y) \exp\left(-\boldsymbol{\lambda}^T \boldsymbol{\phi}(y)\right) dy. \tag{8}$$

III. Proposed Maximum-Entropy Implementation

A. Selections of the Constraint Functions

1) Numerical Stability Issues: A popular choice in existing literature is $\phi_j(y) = y^j$, since μ_j can be computed easily as an empirical statistical moment from the measurement/simulation data. However, this choice can make the algorithm numerically unstable. In order to show this, let us assume that $\boldsymbol{\lambda}$ is very close to the exact solution, and thus

$$\mathbf{J}_{j,k}\left(\boldsymbol{\lambda}\right) \approx -\mathbb{E}\left(\phi_{j-1}(y)\phi_{k-1}(y)\right) = -\mathbb{E}\left(y^{k+j-2}\right), \tag{9}$$

which is very close to the $(j+k-2)$-th moment. Very often, the elements at the left-upper part of $\mathbf{J}\left(\boldsymbol{\lambda}\right)$ are very small, and those at the right-lower part are extremely large (or vice versa), leading to an ill-conditioned Jacobian.

2) Our Choice of $\phi_j(y)$: In order to make the Newton's iterations more robust, we propose to use a set of orthonormal polynomials $\{\phi_j(y)\}_{j=0}^m$. Specifically, $\phi_j(y)$ is a degree-j polynomial subject to the constraint:

$$\mathbb{E}\left(\phi_j(y)\phi_k(y)\right) = \delta_{j,k} = \begin{cases} 1, \text{ if } j = k, \\ 0, \text{ otherwise.} \end{cases} \tag{10}$$

Accordingly, we set $\mu_0 = 1$ and $\mu_j = 0$ for $j \geq 1$ in (4).

The orthonormal polynomials $\{\phi_j(y)\}_{j=0}^m$ can be constructed via the following two steps [18]. Step 1: construct a set of orthogonal polynomials $\{\pi_j(y)\}_{j=0}^m$ according to

$$\pi_{j+1}(y) = \left(y - \gamma_j\right)\pi_j(y) - \kappa_j \pi_{j-1}(y), \ \ j = 0,\ 1, \cdots m-1$$

with initial conditions $\pi_{-1}(y) = 0$, $\pi_0(y) = 1$ and $\kappa_0 = 1$. For $j \geq 0$, the recurrence parameters are defined as

$$\gamma_j = \frac{\mathbb{E}\left(y\pi_j^2(y)\right)}{\mathbb{E}\left(\pi_j^2(y)\right)}, \ \kappa_{j+1} = \frac{\mathbb{E}\left(y\pi_{j+1}^2(y)\right)}{\mathbb{E}\left(y\pi_j^2(y)\right)}. \tag{11}$$

Step 2: obtain $\{\phi_j(y)\}_{j=0}^m$ by normalization:

$$\phi_j(y) = \frac{\pi_j(y)}{\sqrt{\kappa_0 \kappa_1 \cdots \kappa_j}}, \text{ for } j = 0, 1, \cdots, m. \tag{12}$$

Using orthonormal polynomials $\{\phi_j(y)\}_{j=0}^m$ in the optimization problem (4) can improve the numerical stability significantly, because now each element in (9) becomes

$$\mathbf{J}_{j,k}\left(\boldsymbol{\lambda}\right) \approx -\mathbb{E}\left(\phi_{j-1}(y)\phi_{k-1}(y)\right) = -\delta_{j,k}. \tag{13}$$

As a result, $-\mathbf{J}\left(\boldsymbol{\lambda}\right)$ gets close to an identity matrix when $\boldsymbol{\lambda}$ approaches the exact solution. This nice property makes the maximum-entropy flow much more robust.

B. Implementation Details

1) Integration When Computing $\phi_j(y)$: In (11) we need to compute some integrals in the form $\mathbb{E}\left(q(y)\right)$, with $q(y) = \pi_j^2(y)$ or $q(y) = y\pi_j^2(y)$. When $y = g(\mathbf{x})$ is a truncated generalized polynomial-chaos expansion, $q(y)$ is always a polynomial of $\mathbf{x}$. Since the probability density function of y is unknown, we compute the integrals by multi-dimensional Gauss quadrature in the parameter space:

$$\mathbb{E}\left(q(y)\right) = \sum_{i_1=1}^{p} \cdots \sum_{i_d=1}^{p} q\left(g(x_1^{i_1}, \cdots, x_d^{i_d})\right) \prod_{k=1}^{d} w_k^{i_k}. \tag{14}$$

TABLE I
DIELECTRIC PROPERTIES OF TISSUES IN HUMAN TORSO

Tissue name	Relative permittivity	Conductivity [S/m]
Body Fluid	69	1.52
Heart	70	0.9
Lung Inflated	24.7	0.36
Liver	53.5	0.61
Fat	5.63	0.04
Aorta	48.3	0.54
Bone Cortical	13.4	0.08
Duodenum	68.7	0.97
Ovary	61.4	1.15
Cerebro Spinal Fluid	72.7	2.22
Muscle	58.9	0.97
Skin	51.9	0.63
Trachea	45.3	0.61
Blood	64.8	0.99
Spinal Cord	36.9	0.41
Thymus	62.4	0.85
Nerve	43.8	0.41

Here $x_k^{i_k}$ and $w_k^{i_k}$ are the i_k-th Gauss quadrature abscissa and weight of parameter x_k, respectively [19]. When the parameter dimensionality d is small, the above quadrature is easy to implement. When d is large, we utilize the recently developed tensor-train decomposition [20] to compute the integral at the cost of only $O(d)$. The details can be found in [21].

2) Integration Inside Newton's Iterations: In Newton's iterations, we need to compute some integrals in the form

$$\mathbb{I}\left(\hat{q}(y)\right) = \int_{\mathbb{R}} \hat{q}(y) \exp\left(-\boldsymbol{\lambda}^T \boldsymbol{\phi}(y)\right) dy \tag{15}$$

where $\hat{q}(y)$ is $\phi_j(y)$ or $\phi_{j-1}(y)\phi_{k-1}$ when we evaluate $f_j(\boldsymbol{\lambda})$ or $\mathbf{J}_{j,k}(\boldsymbol{\lambda})$, respectively. Let $h(y;\mu,\sigma^2)$ be a Gaussian density function with mean value μ and variance σ^2, then

$$\mathbb{I}\left(\hat{q}(y)\right) = \int_{\mathbb{R}} \tilde{q}(y) h\left(y;\mu,\delta^2\right) dy \tag{16}$$

with $\tilde{q}(y) = \frac{\hat{q}(y)\exp\left(-\boldsymbol{\lambda}^T\boldsymbol{\phi}(y)\right)}{h(y;\mu,\delta^2)}$. Therefore, $\mathbb{I}\left(\hat{q}(y)\right)$ can be evaluated by the existing Gauss-Hermite quadrature rule. In our implementation, we set μ and σ to the mean and variance of y respectively, which can be easily obtained from (1).

IV. NUMERICAL RESULTS

Fig. 1 shows a simplified MRI prototyping model, which suffices for algorithm verification. In this MRI configuration, human torso is represented by a cylindrical scatterer with radius of 10 cm and height of 25 cm illuminated by four loop antennas (radius of 7.5 cm) at the frequency of 300 MHz, placed 20cm away from the center of the cylinder on x, y and z axis. The cylinder contains dielectric inhomogeneities representing different tissues in human torso. The nominal values of the electrical parameters of different tissues in human torso are summarized in Table I. The interaction between electromagnetic waves and biological tissues is evaluated by computing the input impedance of the loop antenna. The basis functions are computed according to the procedures detailed in Section II of [10]. When only Gaussian-type uncertainties

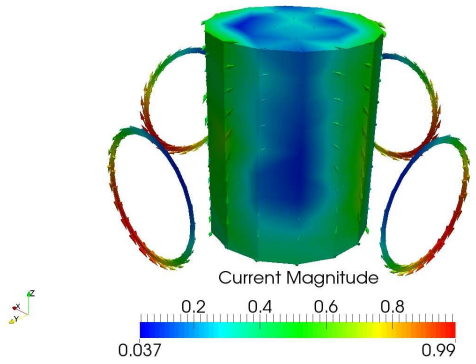

Fig. 1. A simplified MRI configuration consisting of loop antennas illuminating an inhomogeneous cylinder representing human torso

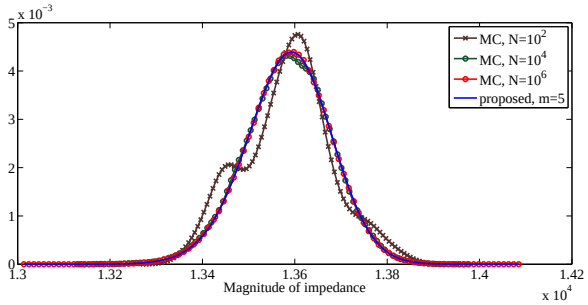

Fig. 2. Probability density function of magnitude of the impedance parameter for the MRI example. Here N is the number of Monte Carlo samples.

are involved, $\Psi_{\boldsymbol{\alpha}}(\mathbf{x})$ simplifies to a normalized multivariate Hermite polynomial.

1) Case 1 (with 10 random parameters): First we consider 10 uncertainties in the electrical permittivity and conductivity of the tissues underlined in Table I. These parameters are assumed Gaussian, with their standard deviations being 15% of their nominal values. We combine the black-box domain-decomposition MRI solver [15] with stochastic testing [7] to obtain a 3rd-order generalized polynomial-chaos expansion for the magnitude of impedance. Six orthonormal polynomials are used (with $m = 5$) to generate a closed-form probability density function of y. Clearly shown in Fig. 2, our result has a similar level of accuracy with that from Monte Carlo using 10^6 samples. Our algorithm requires 18 seconds of CPU time, and it is $36\times$ faster than Monte Carlo.

2) Case 2 (with 34 random parameters): As a higher-dimensional example, 34 random parameters including the electrical permittivity and conductivity of all tissues in human torso in Table I are considered for the same MRI configuration (Fig. 1). All parameters are assumed Gaussian with their standard deviations being 25% of the norminal values. In this example, the ANOVA-based stochastic testing solver [17] is combined with the deterministic MRI solver [15] to obtain a sparse generalized polynomial-chaos expansion for the loop antenna impedance, and the tensor-train-based three-term recurrence relation is employed to construct some orthonormal polynomials [21]. The numerical results are plotted in Fig. 3. With 5 orthonormal polynomials in the constraints, our algorithm has generated a very accurate density function. Note

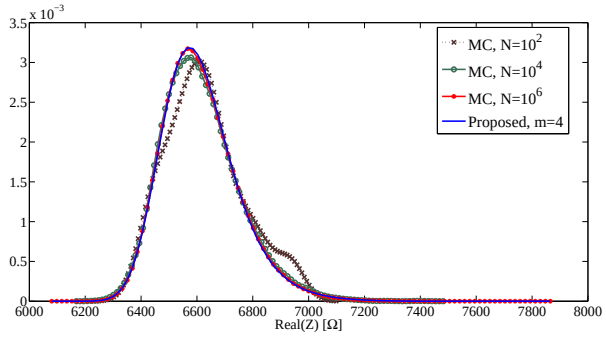

Fig. 3. Probability density function of real part of the impedance parameter for the MRI example. Here N is the number of Monte Carlo samples.

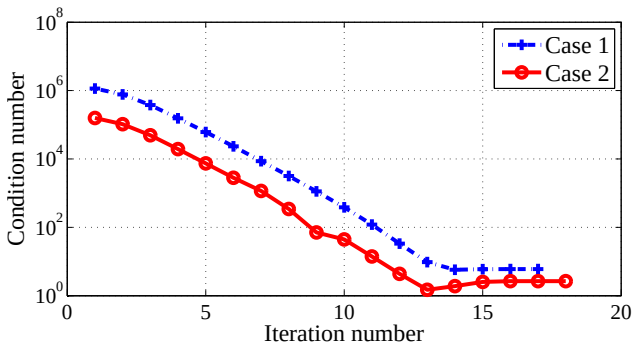

Fig. 4. The condition number of $\mathbf{J}(\boldsymbol{\lambda})$ during Newton's iterations.

that generating the density function with Monte Carlo (using 10^6 samples) needs about 2 hours, while our technique only requires about 30 seconds.

3). Numerical Stability: Fig. 4 shows the condition numbers of the Jacobian matrix $\mathbf{J}(\boldsymbol{\lambda})$ during the Newton's iterations. For both examples, due to the use of orthonormal polynomials in the constraints, the condition number quickly decreases to a small value close to 1. Neither of these examples could be solved if we directly use a set of statistical moments in the constraints, since the condition number of $\mathbf{J}(\boldsymbol{\lambda})$ becomes extremely large and Newton iterations fail to work.

V. Conclusions and Future Work

In this paper we have proposed an implementation that improves the robustness of maximum entropy for estimating the density functions of MRI stochastic surrogate models. We have reduced the condition number of the Jacobian matrix by using the expectations of some orthonormal polynomials as the equality constraints. Our proposed algorithm has been verified on a simplified MRI prototyping model with both low- and high-dimensional random parameters, generating very accurate density functions with dozens to hundreds of times of speedup over Monte Carlo. The improvement of numerical stability has been demonstrated by our numerical results.

It is worth extending the proposed algorithm to the case that y is a non-smooth function of $\mathbf{x}$. In such a case, our current implementation may be unable to construct accurately a set of orthonormal polynomials for y.

References

[1] T. Moselhy and L. Daniel, "Variation-aware stochastic extraction with large parameter dimensionality: Review and comparison of state of the art intrusive and non-intrusive techniques," in *Proc. Intl. Symp. Quality Electronic Design*, Mar. 2011, pp. 1–16.
[2] A. C. Yücel, Y. Liu, H. Bağc, and E. Michielssen, "Statistical characterization of electromagnetic wave propagation in mine environments," *IEEE Antennas Wireless Propag. Lett.*, vol. 12, pp. 1602–1605, 2013.
[3] C. Chauviere, J. S. Hesthaven, and L. C. Wilcox, "Efficient computation of RCS from scatterers of uncertain shapes," *IEEE Trans. Antennas Propag.*, vol. 55, no. 5, pp. 1437–1448, 2007.
[4] A. C. M. Austin and C. D. Sarris, "Efficient analysis of geometrical uncertainty in the FDTD method using polynomial chaos with application to microwave circuits," *IEEE Trans. Microw. Theory Techn*, vol. 62, no. 6, pp. 4293 – 4301, 2013.
[5] D. Xiu and G. E. Karniadakis, "The Wiener-Askey polynomial chaos for stochastic differential equations," *SIAM Journal on Scientific Computing*, vol. 24, no. 2, pp. 619–644, Feb 2002.
[6] D. Xiu, "Fast numerical methods for stochastic computations: A review," *Comm. in Comput. Phys.*, vol. 5, no. 2-4, pp. 242–272, Feb. 2009.
[7] Z. Zhang, T. A. El-Moselhy, I. M. Elfadel, and L. Daniel, "Stochastic testing method for transistor-level uncertainty quantification based on generalized polynomial chaos," *IEEE Trans. CAD Integr. Circ. Syst.*, vol. 32, no. 10, pp. 1533–1545, Oct 2013.
[8] D. Voyer, F. Musy, L. Nicolas, and R. Perrussel, "Probabilistic methods applied to 2D electromagnetic numerical dosimetry," *Int. J. Comput. Math. Electr. Electron. Eng.*, vol. 27, no. 3, pp. 651–667, 2008.
[9] S. Mookherjea, "Spectral characteristics of coupled resonators," *J. Opt. Soc. Am. B*, vol. 23, no. 6, pp. 1137–1145, 2006.
[10] Z. Zhang, I. M. Elfadel, and L. Daniel, "Uncertainty quantification for integrated circuits: Stochastic spectral methods," in *Proc. Int. Conf. Computer-Aided Design*. San Jose, CA, Nov 2013, pp. 803–810.
[11] X. Li, J. Le, P. Gopalakrishnan, and L. T. Pileggi, "Asymptotic probability extraction for non-normal distributions of circuit performance," in *Proc. Int. Conf. Computer-Aided Design*, Nov 2004, pp. 2–9.
[12] Z. Zhang, T. A. El-Moselhy, I. M. Elfadel, and L. Daniel, "Calculation of generalized polynomial-chaos basis functions and gauss quadrature rules in hierarchical uncertainty quantification," *IEEE Trans. CAD of Integr. Circ. Syst.*, vol. 33, no. 5, pp. 728–740, May 2014.
[13] C. E. Shannon, "A mathematical theory of communication," *The Bell Systems Technical Journal*, vol. 27, pp. 379–423, July 1948.
[14] R. Krishnan, W. Wu, F. Gong, and L. He, "Stochastic behavioral modeling of analog/mixed-signal circuits by maximizing entropy," in *Proc. Intl. Symp. Qual. Electr. Design*. Santa Clara, CA, Mar 2013, pp. 572–579.
[15] N. Farnoosh, A. G. Polimeridis, T. Klemas, and L. Daniel, "Accelerated domain decomposition FEM-BEM solver for magnetic resonance imaging (MRI) via discrete empirical interpolation method," in *Int. Symp. VLSI DAT*. Taiwan, May 2014.
[16] A. Hochman, J. F. Villena, A. G. Polimeridis, J. K. White, and L. Daniel, "Reduced-order models for electromagnetic scattering problems," *IEEE Trans. Antennas Propag.*, vol. 61, no. 12, pp. 3150 – 3162, June 2014.
[17] Z. Zhang, X. Yang, G. Marucci, P. Maffezzoni, I. M. Elfadel, G. Karniadakis, and L. Daniel, "Stochastic testing simulator for integrated circuits and MEMS: Hierarchical and sparse techniques," in *Proc. IEEE Custom Integrated Circuits Conf.* San Jose, CA, Sept. 2014.
[18] W. Gautschi, "On generating orthogonal polynomials," *SIAM J. Sci. Stat. Comput.*, vol. 3, no. 3, pp. 289–317, Sept. 1982.
[19] G. H. Golub and J. H. Welsch, "Calculation of gauss quadrature rules," *Math. Comp.*, vol. 23, pp. 221–230, 1969.
[20] I. V. Oseledets, "Tensor-train decomposition," *SIAM J. Sci. Comput.*, vol. 33, no. 5, pp. 2295–2317, 2011.
[21] Z. Zhang, I. Osledets, X. Yang, G. E. Karniadakis, and L. Daniel, "Enabling high-dimensional hierarchical uncertainty quantification by ANOVA and tensor-train decomposition," arXiv:1407.3023.